Production and Recovery of Electron-Induced Radiation Damage in a Number of Metals*†

P. G. LUCASSON‡ AND R. M. WALKER
General Electric Research Laboratory, Schenectady, New York

(Received March 12, 1962)

The changes in residual electrical resistance produced by bombardment with high-energy electrons were measured for a number of metals as a function of electron energy in the range from 0.5 to 1.4 MeV. The irradiations were performed at $\lesssim$20°K, and recovery measurements were made up to 300°K. The production curves were analyzed using simple displacement theory and the following values were found for the average threshold energies: Al, 32 eV; Au, >40 eV; Ag, 28 eV; Cu, 22 eV; Fe, 24 eV; Mo, 37 eV; Ni, 24 eV; Ti, 29 eV; and W, >35 eV. Approximate values for the resistivities of Frenkel pairs (in units of $\mu\Omega$ cm per at. %) were also obtained as follows: Al, 3.4; Ag, 1.4; Cu, 1.3; Fe, 12.5; Mo, 4.5; Ni, 3.2; and Ti, 42. In the case of Al it was necessary to take secondary defect production into account and a number of representative theoretical curves, based on different assumptions concerning the process of secondary defect production, are included. The behavior of Zn was anomalous in that the added resistivity was not a linear function of electron dose at 20°K.

I. INTRODUCTION

PRIOR studies of the production and recovery of radiation damage in electron-bombarded copper have given considerable information about the displacement of atoms and the properties of simple lattice defects in this material.[1] This paper is concerned with similar studies in a number of other metallic elements. The objective of this work was to obtain an over-all view of radiation damage in metals and in particular to compare the results for other metals with those for copper.

Specifically, we report here measurements of the change in residual electrical resistance as a function of bombarding electron energy in the range from 0.5 to 1.4 MeV. The following elements were studied: Al, Ag, Au, Cu, Fe, Mo, Ni, Ti, W, and Zn. No damage was observed in Au and W and only limiting values can be set for these elements. Most of the irradiations were performed at 20°K, although some were done at a lower temperature. The recovery was followed by annealing experiments up to room temperature.

Electron bombardments have two unique advantages for studying radiation damage, both of which stem from the low recoil energy which is transmitted to the lattice atoms. Firstly, the energy transfers are so low that, in general, only isolated Frenkel pairs are created. Thus the observed property changes are related directly to the properties of these fundamental point defects. A second advantage is that the electron energy can be lowered to the point where damage just starts to occur. In this way the threshold region of the displacement process can be studied.

The remainder of this paper is divided into four sections. The first three of these deal, respectively, with the experimental procedures, the numerical treatment of the raw data, and the experimental results. The fourth section deals with the comparison of the results with radiation damage theory. From this comparison it is possible to determine "effective" threshold energies and approximate values for the resistivities of Frenkel pairs. With the exception of Zn and Al, all the elements for which production data were obtained were found to fit simple displacement functions. In the case of Al it was necessary to take into account secondary defect production in order to fit the data. A number of calculations for different models of the secondary production process are presented in the discussion of the Al data. These calculations show how production curves change when secondary defect production becomes important. Zinc exhibited an anomalous behavior in that the resistivity change was a highly nonlinear function of dose at 20°K.

In a subsequent paper we will discuss some of the implications of the present results.

II. EXPERIMENTAL

The experiment consisted of determining the change in electrical resistance in irradiated thin metal foils. In this section we describe the specific experimental procedures.

The irradiated samples were thin strips of metal about 1-in. long, 0.030-in. wide, and 0.001-in. thick.

All the samples, except aluminum, were obtained by cold-rolling in specially cleaned rollers to the desired thickness. They were etched between each rolling pass, and after the final rolling they were given a high-temperature, vacuum anneal.

The silver sample was rolled from a piece of a single crystal grown from a starting material obtained from the Consolidated Mining and Smelting Company of Canada. The stated purity of this starting material was 99.9999%. The sample was annealed in vacuum at 350°C for 12 h. The resistivity ratio from 0°C to 4.2°K was 185. This relatively low ratio indicates that the

* The research reported in this paper was sponsored by the Electronics Research Directorate of the Air Force Cambridge Research Center, Air Research and Development Command.

† A partial account of this work was given in the Discussions Faraday Soc. 31, 57 (1961).

‡ Permanent address: Laboratoire de Chimie Physique, Faculté des Sciences de Paris, Orsay (Seine et Oise), France.

[1] For a recent review see R. M. Walker, Nuovo cimento (to be published).

purity of the final sample was not as high as the stated purity of the starting material.

The copper samples were rolled from a section of a single crystal of copper obtained from the Virginia Institute of Scientific Research. These foils were vacuum annealed for 12 h at 450°C. The ratio of the resistivity at 0°C to that at 4°K was 400.

The iron and nickel samples were prepared from spectroscopically pure sheets obtained from the Johnson-Matthey Company. They were vacuum annealed overnight, the iron at 450°C and the nickel at 600°C. The resistivities ratios from 0°C to 20.4°K were 110 for the iron and 26 for the nickel.

The aluminum sample was a 0.014-in. diameter wire drawn from zone-refined material and was from the same batch that DeSorbo and Turnbull[2] used in their quenching experiments. The stated purity of the material before zone-refining was 99.99+%. The ratio of the resistance at 273°K to that at 20.4°K was 730.

The molybdenum sample was prepared from an ingot of arc-melted material. The stated purity of the molybdenum, before arc melting, was 99.9+%. This sample was vacuum annealed at 1100°C for 1 h and then slowly cooled. The ratio of resistance at 0°C to that at 4.2°K was 95.

The zinc sample was prepared from a bar of zone-refined material and was not given any heat treatment after rolling. The ratio of resistance at 0°C to that at 4.2°K was 410.

The titanium sample was prepared from material which was formed by the reduction of iodide titanium. The stated purity of the starting material was 99.97%. The rolled specimens were vacuum annealed at 800°C for 30 min. The ratio of resistance at 0°C to that at 4.2°K was only 3.9 and it is apparent that the annealing treatment was not sufficient to soften the material.

The tungsten sample was the most impure of any of the elements studied. It was formed from a sheet of number 218 "shelf" grade tungsten obtained from the General Electric Company. The foil was vacuum annealed at 1000°C for 2 h and had a ratio of resistance at 273°K to that at 4.2°K of 26.

Current and potential leads were soldered directly to the samples for the elements Al, Ni, Cu, Fe, Ag, Au, and Zn. In the case of Mo, W, and Ti the nonirradiated ends were first plated, and the leads then soldered in position.

Transmission x-ray patterns were taken of all the foils to make sure that they were polycrystalline and that they lacked preferred orientation. The grain size varied for different elements but was typically about 1×10^{-3} cm. Some slight preferred orientation was observed in several cases, but our experience with single crystals leads us to believe that the small amount observed should not affect the results.

These thin strips were clamped to insulated metal bars at each end and the central portion hung freely between these end supports. Only this central section was irradiated. The samples were mounted and tested in a separate holder which could be attached to the irradiation cryostat in a few minutes. Each sample holder contained two thermocouples and a carbon resistor to monitor temperature. Three irradiation and three control samples were mounted in a single holder, thereby permitting three different materials to be studied in a single irradiation. A total of four sample holders was used in these experiments. The first contained copper, iron, and nickel. The second contained copper, aluminum, and silver. The third contained molybdenum and tungsten, and the final assembly held zinc and titanium. The gold data were obtained in an earlier experiment[3] and are included here for completeness. There were two specimens (irradiated and control) of each element.

Two potential leads were connected to each sample and the potential difference was measured with a Rubicon 6-dial potentiometer. A precision of ±0.01 μV was obtained after thermal insulation of all contacts. The samples were connected in series and the measuring current of 300 mA was automatically regulated to about $\frac{1}{10^5}$. The effects of thermal emf's were eliminated by taking forward and reverse current readings for all points. The additional resistivities added by irradiation were calculated from the changes in the difference readings between the irradiated and control samples.

The irradiation cryostat consisted of a conventional cylindrically symmetric liquid refrigerant container with a projecting side arm. The sample holder was mounted in this side arm and the samples were cooled by pumping the refrigerant past the samples in the manner described by Corbett, Denney, Fiske, and Walker.[4] In this apparatus, the irradiated portions of the samples were completely surrounded by the refrigerant. Liquid hydrogen was used as the refrigerant in most of the present experiments.

The electron accelerator was a conventional G.E. resonant transformer with a gated beam output. The beam current was turned on from 0° to 32° of a voltage cosine wave. Absolute calibration of the peak voltage was done by measuring the onset of neutron production from the Be(γ,n) threshold reaction at 1.665 MeV. This calibration was carried out immediately prior to the present set of experiments. The results agreed with a similar calibration performed about five years ago. The calibration constant also agreed within 2% with a spark gap measurement performed at 100 keV. In this machine the charging current is proportional to the peak voltage. This current was carefully monitored during a run. A numerical analysis of the current-voltage characteristic gives an average energy of the

[2] W. DeSorbo and D. Turnbull, Phys. Rev. **111**, 810 (1958); **115**, 560 (1959).

[3] J. W. Corbett and R. M. Walker, Phys. Rev. **117**, 970 (1960).

[4] J. Corbett, J. Denney, M. Fiske, and R. Walker, Phys. Rev. **108**, 4, 954 (1957).

electrons 0.95 times the peak value. There is $\pm 1.5\%$ uncertainty in the accuracy of the peak energy and $\pm 2.5\%$ uncertainty in the average energy of the internal accelerator beam.

In going from the interior of the accelerator to the surface of the samples, the electron beam passed through the following material: 22.5 mg/cm^2 of Ti, 4.4 mg/cm^2 of air, 44.6 mg/cm^2 of Be, and 8 mg/cm^2 of liquid hydrogen. The analysis of the resulting beam energy and directional distribution is dealt with in the following section.

The sample area illuminated by the beam was defined by an opening $\frac{3}{8}$-in. long by $\frac{3}{16}$-in. wide which was cut in a 0.020-in. thick piece of Pt suspended immediately above the samples. The current density was found to vary considerably in this illuminated region and it was necessary to determine the current density at the position of the different samples at each bombarding energy. These values were obtained by replacing the sample holder with a Faraday cage whose entrance aperture was defined by a slot cut in a platinum insert. Several platinum inserts were constructed whose slot widths were equal to the sample widths and whose positions corresponded to the sample positions. By measuring the current delivered to the Faraday cage with a fixed internal-machine current, a calibration curve of current density versus energy was constructed for each sample. In order for this procedure to be valid, the spatial distribution of the beam with respect to the cryostat must be the same during the calibration and subsequent sample irradiation experiments. A beam centering device was constructed to insure that this was the case, and it was found that the calibration curves, taken before and after each of the sample irradiations, were reproducible within $\pm 1.5\%$.

Platinum inserts with slots of identical width but different lengths were used to check the "fuzziness" of the beam defined by the entrance aperture. Inserts containing slots of identical length but different widths were used to check whether the geometric width and "effective" width of the narrow slots were identical. The samples and the corresponding beam measuring slots were located with respect to the fixed entrance aperture with an accuracy of 0.001 in. The slots themselves were measured with an accuracy of 0.0002 in. Current values were measured by determining the voltage drop across a 100 kΩ resistance with a filtering capacitance of 10 μF. The sample current densities were about 2 μA/cm^2 and the absolute accuracy of the overall measuring procedure is estimated as better than 3%.

III. DATA ANALYSIS

The experiments consisted of determining the change of voltage across the samples following irradiation at certain accelerator settings. This section describes how the raw data obtained in this way can be used, finally, to study the variation in atomic displacement cross sections of the irradiated materials as a function of bombarding electron energy.

The conversion of voltage changes into resistivity values is considered first. The relationship between such resistivity changes and the cross sections for defect production is then discussed for the simple case of an ideally thin sample. The case with a finite sample thickness is then considered. This discussion takes into account the effects of angular deviation due to elastic scattering. Because of this scattering the average path length of the electrons is greater than the sample thickness. This scattering also causes an inhomogeneous distribution of damage.

The problem of determining the beam energy is considered next. Even inside the accelerator vacuum the internal accelerator beam is not monoenergetic. As the beam passes successively through several thin windows and then through the samples, its distribution in energy becomes still wider and shifts asymmetrically toward low energies. As a first approximation, we assume that the effect of the actual beam is identical to that of monoenergetic electrons with an energy equal to the *average* beam energy. The method of calculating this average beam energy is first described, following which a more rigorous treatment of the distribution of beam energies is given.

The last part of this section discusses the effect of boundary scattering on the measured resistivity changes.

a. Determination of Experimental Resistivity Change

Consider a foil of width W, thickness t_0, and total length L_0. If a segment of length L_i is irradiated uniformly with a beam of electrons, and if the damage is homogeneously distributed throughout the thickness of the foil, then the change in resistivity per electron per cm^2 is given by

$$(\Delta\rho/n)_e = (Wt_0/L_i n)(\Delta R), \tag{1}$$

where ΔR is the measured resistance change and n is the measured current density. In our experiments W is measured with a traveling microscope, and t_0 is determined by weighing a measured area of the sample foil. These values are checked by comparing the room temperature resistivity values with handbook tabulations.

As previously described, the beam striking the sample is limited by a platinum aperture immediately above the sample. If this aperturing arrangement were perfect, then L_i would be simply the measured slit length in the platinum aperture. In fact, the collimation is not perfect and some electrons coming through the slit at wide angles strike the samples beyond the ends of the aperture. We take this into account by defining an effective L_i which can be measured by using beam measuring slits of different length. This effective length was never

more than 5% larger than the measured slit length in the beam defining aperture.

b. Relationship of Displacement Cross Section to Resistivity Measurements

In this section we discuss how experimental resistivity measurements can be used to obtain information about the cross sections for atomic displacement. We will assume that the foils employed are sufficiently thin so that no angular deviation or energy degradation of the beam occurs. In practice, both effects are important and are taken into account in succeeding sections.

In the case of a very thin sample with a beam of electrons incident normal to the surface, the concentration of the i type of defect is given by

$$D_i = n\sigma_i, \tag{2}$$

where σ_i is the cross section for defect production and n is the total number of electrons per unit area striking the foil. The corresponding increase in resistivity is given by

$$\Delta\rho = n\sum_i \sigma_i \Delta\rho_i, \tag{3}$$

where $\Delta\rho_i$ is the resistivity increment per unit concentration of defects. The first assumption which we make is that only one type of defect is formed and hence that we can drop the summation and subscripts in Eq. (3), and write instead

$$\Delta\rho = n\sigma\Delta\rho_f. \tag{4}$$

This assumption is not strictly correct. As shown by Corbett, Smith, and Walker,[5] for the case of copper, several distinct types of defects are formed at a given bombarding energy. However, it will turn out that we are mostly interested in the variation of the resistivity change with bombarding energy. Since Corbett and Walker[6] have shown that approximately the same distribution of defects results over a wide range of bombarding energies, it is reasonable to work with Eq. (4) and treat $\Delta\rho$ as arising from a unique defect. Further, the different defects which are formed are simply Frenkel pairs with differing separations between the interstitials and vacancies. These different pairs are not expected to have widely different resistivities, and $\Delta\rho_f$ is therefore assumed to be the resistivity of a unit concentration of Frenkel pairs in which the interstitials and vacancies are widely separated.

In Eq. (4) $\Delta\rho$ and n are experimental numbers while σ is the quantity which is computed by damage theory and which we would like to check experimentally. In general, $\Delta\rho_f$ is not known and its presence complicates the comparison between theory and experiment. In order to eliminate $\Delta\rho_f$, we normalize the results at a particular energy E_0 and compare $(\Delta\rho/n)_E/(\Delta\rho/n)E_0$ with $\sigma(E)/\sigma(E_0)$. Thus, such a comparison tests only the dependence of σ on E. The implications of this procedure are discussed in the next part of this paper.

c. Inclusion of Angular Deviation Effects

In the above discussion we assumed an infinitely thin foil through which the electrons passed without deviation. Actually, the electrons are deflected many times by elastic scattering. As a result there is a statistical distribution of electron directions about the initial direction of the beam. This scattering has the following effects. Firstly, when an electron arriving perpendicularly to the surface is scattered, its path length in the foil is increased—thus both the probability of losing energy and creating defects in the foil increase. Also, because the average angular deviation is a function of penetration depth, the damage is not produced homogeneously through the body of the specimen. Finally, some electrons are scattered out of the sides of the foil before they penetrate completely, thus producing less damage in the bulk of the specimen. Explicit calculations show that this last effect is negligible for the foils used in this experiment and it will not be discussed further. The effect on the energy loss will be considered later. The other effects are treated in more detail below.

Consider first the difference δ between the average path length and the foil thickness. Yang[7] has derived two expressions for δ in the case of electrons incident normally on a thin foil of thickness t. If only electrons which emerge parallel to the incident beam are considered, Yang gives

$$\delta = t^2/3\omega^2, \tag{5}$$

where ω is the electron energy and t is expressed in radiation lengths. If electrons emerging at all angles are counted, then

$$\delta = t^2/\omega^2. \tag{6}$$

The *average* concentration of defects produced in the foil is now given by

$$\bar{D} = (1+\delta/t)n\sigma = (1+Kt)n\sigma, \tag{7}$$

where $K = 1/\omega^2$.

Experimentally, it is the resistance change and not the average defect concentration which is measured. Because the defects are not distributed uniformly through the specimen, there is not a linear relationship between these quantities; i.e., there is no simple analog to Eq. (4). However, as we shall now show, for most cases of practical interest, an analogous expression is valid. Consider a thin slab of material of width W, length L, and thickness t_0. Current and potential leads are attached at the ends of the specimen and a uniform electron beam is perpendicular to the thin dimension of the slab. If L and W are sufficiently large, then the added defect resistivity $\Delta\rho$ will be uniform throughout a thin section of length L, width W, and thickness dt,

[5] J. Corbett, R. Smith, and R. Walker, Phys. Rev. **114**, 6 (1953).
[6] J. Corbett and R. Walker, Phys. Rev. **115**, 560 (1953).
[7] C. N. Yang, Phys. Rev. 84, 599 (1951).

but will be a function of t. Before irradiation the residual resistivity is ρ_0. After irradiation it is $\rho_a=\rho_0+\Delta\rho(t)$. The resistance before irradiation is simply

$$R_b=L\rho_0/Wt. \tag{8}$$

After irradiation the situation is more complicated. In this case the resistance is given by the inverse of the total conductance, C, as follows:

$$R_a=\left[\frac{W}{L}\int_0^{t_0}C(t)dt\right]^{-1}=\left[\frac{W}{L}\int_0^{t_0}[\rho_0+\Delta\rho(t)]^{-1}dt\right]^{-1}. \tag{9}$$

The change in resistance is then given by

$$\Delta R=\left\{\left[\int_0^{t_0}[\rho_0+\Delta\rho(t)]^{-1}dt\right]^{-1}-\rho_0/t_0\right\}\frac{L}{W}. \tag{10}$$

The apparent or "experimental" change in resistivity is defined as

$$\Delta\rho_e\equiv\frac{Wt_0}{L}[\Delta R]=t_0\rho_0\left\{\left[\int_0^{t_0}(1+\Delta\rho/\rho_0)^{-1}dt\right]^{-1}-t_0^{-1}\right\}. \tag{11}$$

In order to find a relationship between $\Delta\rho_e$ and the cross section for displacement, we must obtain an explicit relation for $\Delta\rho(t)$. Consider a slab of thickness dt at a distance t from the surface. The concentration of defects produced in the slab if the beam went through perpendicularly would be simply $n\sigma$, and the resistivity increase would be $n\sigma\Delta\rho_f$. From Eq. (6) it is easy to show that the actual average path length in this thin slab is equal to $(1+2Kt)dt$. The resistivity increase $\Delta\rho(t)$ is therefore

$$\Delta\rho(t)=(1+2Kt)n\sigma\Delta\rho_f=(1+2Kt)\Delta\rho_i, \tag{12}$$

where we have replaced $n\sigma\Delta\rho_f$ by $\Delta\rho_i$ for convenience. Substituting Eq. (12) in Eq. (11) and solving, we have finally

$$\Delta\rho_e=\frac{2Kt\Delta\rho_i-\rho_0\ln\{[1+\Delta\rho_i/\rho_0+2Kt\Delta\rho_i/\rho_0][1+\Delta\rho_i/\rho_0]^{-1}\}}{\ln\{[1+\Delta\rho_i/\rho_0+2Kt\Delta\rho_i/\rho_0][1+\Delta\rho_i/\rho_0]^{-1}\}}. \tag{13}$$

Let us consider two limiting cases. Firstly, the most common situation is where $\Delta\rho_i\ll\rho_0$. This is the case which is valid for the experiments performed here. Expanding Eq. (13) and passing to the limit as $\rho_0\to\infty$, we find

$$\Delta\rho_e=[1+Kt]\Delta\rho_i. \tag{14}$$

Hence

$$\sigma=(\Delta\rho/n)_e[(1+Kt)\Delta\rho_f]^{-1}=(\Delta\rho/n)_e(\Delta\rho_f)^{-1}, \tag{15}$$

where

$$(\Delta\rho/n)_e\equiv(\Delta\rho/n)_e(1+Kt)^{-1}. \tag{16}$$

The other limiting case is where $\Delta\rho_i\gg\rho_0$. For this case we find

$$\sigma=(\Delta\rho/n)_e(2Kt\Delta\rho_f)^{-1}\ln(1+2Kt). \tag{17}$$

This equation was incorrectly given in an earlier paper[8] as having general validity. However, Eq. (17) reduces to Eq. (15) in the limit where kt is small and in the experiments described here there is little numerical difference between Eq. (17) and Eq. (15).

The net results of the foregoing analysis can be stated as follows: If the initial resistivity of the specimen is much larger than the radiation-induced change, or if $\delta/t_0\ll1$, then the apparent resistivity change has to be corrected by the ratio of the average path length to the thickness in order to get a number proportional to the displacement cross section. If the radiation-induced change is much larger than the initial resistivity, and if the increase in path length is a large fraction of the thickness, then Eq. (17) must be used.

The above equations were derived on the assumption that the incident beam was normal to the foil. In our experiments there is a layer of liquid hydrogen and a Be window immediately above the samples. Thus the electrons striking the sample are already scattered and do not all enter perpendicularly. This is taken into account in the following way: Consider a sandwich of two absorbers of thickness t_1 and t_2, respectively. The ratio δ/t_2 in the second absorber is given by

$$(\delta_2/t_2)=(\delta_1/t_1)(t_2/t_1+2)=Kt_2. \tag{18}$$

The subscript 1 refers to the Be window plus liquid hydrogen while the subscript 2 refers to the sample. This equation is then used to calculate values of Kt_2 for insertion in Eq. (15). We assume that the electrons are incident normally on the Be window. This is not strictly true since the Ti entrance window above the Be also scatters the electrons. However, this window is sufficiently thin and sufficiently far removed from the Be window so that this is a reasonable approximation.

The scattering correction outlined above constitutes the major correction to the experimental data. Unfortunately, this correction is somewhat uncertain. Hebbard and Wilson[9] and McDonnell, Hanson, and Wilson[10] have made theoretical and experimental studies of electron energy losses in various absorbers. They conclude that an average increase in path length about one-half that given by Yang [Eq. (6)] gives the

[8] P. Lucasson and R. M. Walker, Discussions Faraday Soc. **31**, 57 (1961).

[9] D. F. Hebbard and P. R. Wilson, Australian J. Phys. **8**, 90 (1955).

[10] J. M. MacDonnell, M. A. Hanson, and P. R. Wilson, Australian J. Phys. **8**, 98 (1955).

best agreement with experiment. Examination of their data indicates that, at high absorber thicknesses (corresponding to values used in this experiment), the actual value lies between $\frac{1}{2}$ to 1 times the full Yang value. In our analysis we have compromised by assuming that δ is 0.75 the value given by Eq. (6). The uncertainty of $\pm 0.25\delta$ is small enough so that none of the conclusions of this paper would be drastically altered by drawing the final curves through the limiting values.

d. Determination of Average Beam-Energy

The purpose of these experiments is to measure the variation in displacement cross section as a function of bombarding electron energy. As previously stated, the internal accelerator beam possesses a distribution of energies. This distribution becomes broader as the beam passes successively through several thin absorbers before reaching the samples. As a first approximation we assume that the effect of the external beam is identical to that of monoenergetic electrons with an energy equal to the *average* energy of the actual beam midway through the sample. Thus this *average* energy is used as the variable in plotting the energy dependence of the resistivity change. This section describes the procedure for calculating this average beam energy. In a later section we discuss a more exact procedure which explicitly includes the energy distribution function. It turns out that the more exact method gives results which are very close to those obtained using the average energy as calculated below. As a result, the simpler procedure is actually used for most of the samples.

The average beam energy midway through the samples is taken as

$$\bar{E}=\bar{E}_{it}-\langle \Delta E\rangle_{\mathrm{av}}, \tag{19}$$

where $\bar{E}_{it}$ is the average energy of the internal accelerator beam and $\langle \Delta E\rangle_{\mathrm{av}}$ is the average energy loss in reaching the middle of the sample. As previously noted, the accelerator is a resonant transformer with the beam gated on during a part of the voltage cycle. The beam current is not quite uniform during the on time and a numerical integration of the beam current-voltage characteristic was performed in order to determine $\bar{E}_{it}$. An average energy loss was calculated from the standard formula.[11] In order to obtain $\langle \Delta E\rangle_{\mathrm{av}}$ we multiplied the absorber thickness by the correction factor K, to take into account the difference δ between the average path length and the foil thickness. A numerical iterative procedure was also used to take into account the change in $\langle \Delta E\rangle$ in traversing the set of absorbers.

Values of average beam energy calculated this way agreed within 30 keV with previous calorimeter measurements of average energy[3] at both low and high energies.

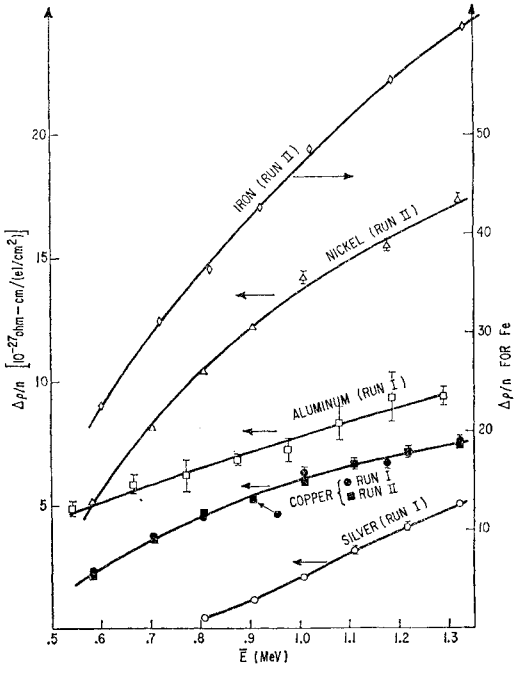

FIG. 1. Experimental results. Resistivity changes per electron/cm² in various specimens against average bombarding electron energy. The resistivities are determined from Eq. (1) of text and do not include corrections for multiple scattering or energy straggling. As described in the text, the determination of average energy includes the multiple scattering correction. Note the different resistivity scales for various elements.

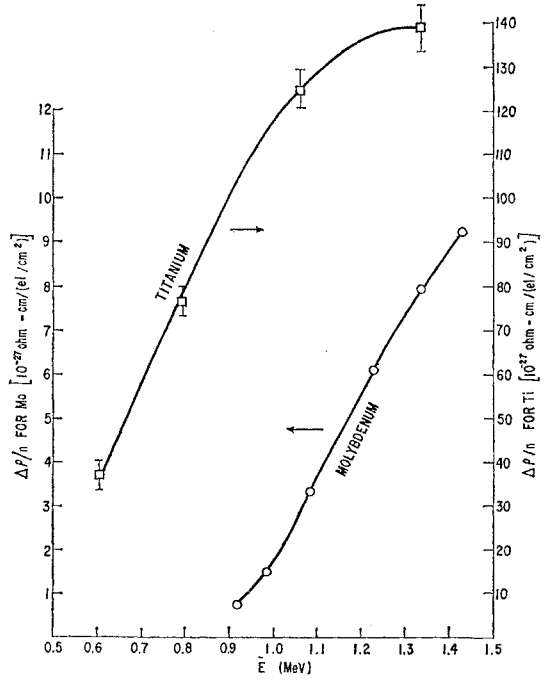

FIG. 2. Same as Fig. 1 for Mo and Ti.

[11] L. Landau, J. Phys. (U.S.S.R.) 8, 201 (1944).

e. Energy Distribution Correction

When an initially monoenergetic beam traverses an absorber, it emerges with a distribution of energies. The distribution is asymmetric and has a long tail extending to low energies. When the average energy is close to that for the onset of damage, the existence of this distribution has two effects. Firstly, electrons in the low-energy tail are still counted by the beam measuring device but can no longer produce damage. These electrons should be subtracted from the total, raising the value of $(\Delta\rho/n)$. Secondly, excluding electrons with energies below threshold, increases the calculated average energy of the remaining electrons. The corrected value of $(\Delta\rho/n)$ should, therefore, be plotted at a higher energy. Detailed numerical calculations for Cu and Ag indicate that the shifts in $(\Delta\rho/n)$ and $\bar{E}$ are small for the present experimental arrangement. The shifts also tend to compensate for one another and the final curve of resistivity as a function of energy remains virtually unchanged. Because explicit calculation showed little effect for Cu and Ag, this distribution correction was not calculated for the other elements.

The detailed calculation for Cu and Ag proceeded as follows: Firstly, the internal accelerator beam was divided into a number of small energy intervals. The energy distribution function resulting from the passage of the beam through the sample and the windows above the sample was then calculated for each of these incident energy intervals. The curve of $(\Delta\rho/n)_c$ vs $\bar{E}$ was then extrapolated to zero to obtain a first approximation

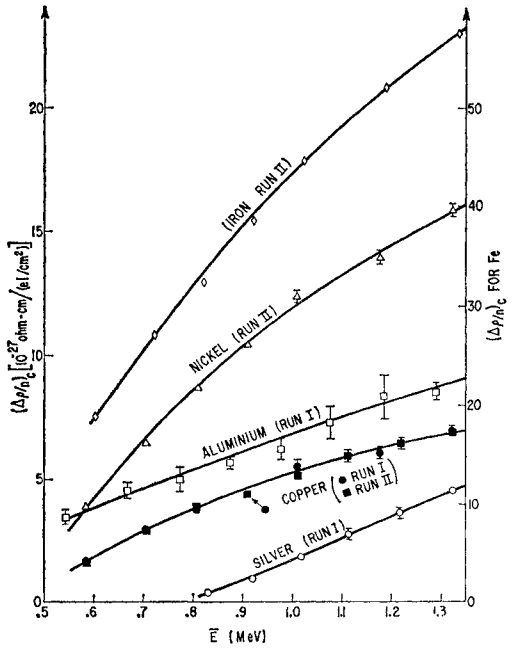

FIG. 3. Corrected values for resistivity changes per electron/cm² including the increase in path length due to multiple scattering. A correction for energy straggling is also included in the case of Cu and Ag. Note the different resistivity scales for various elements.

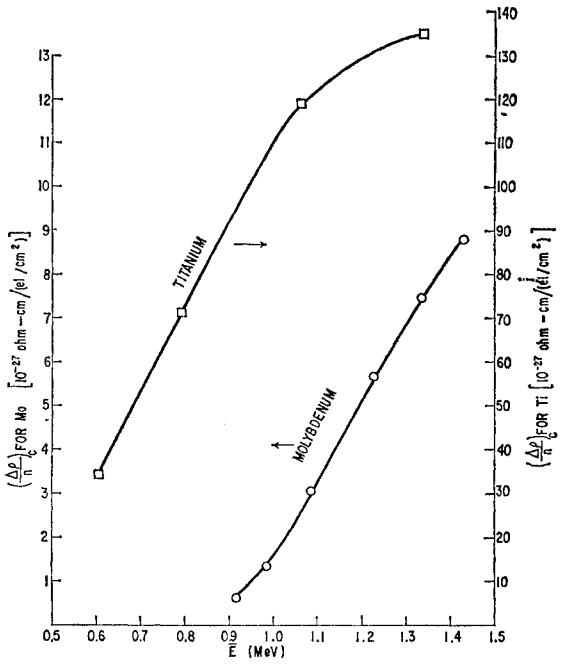

FIG. 4. Same as Fig. 3 for Mo and Ti.

for the threshold energy. The distribution functions were then cutoff at this energy and the $(\Delta\rho/n)_c$ and average values were recalculated. A new curve of $(\Delta\rho/n)_c$ vs $\bar{E}$ was then constructed and the process was repeated. This procedure gave a rapid convergence.

The energy distribution functions were calculated from Landau's[11] theory including the scattering correction in the manner described by Hebbard and Wilson.[8]

f. Boundary Scattering Correction

As previously noted by Corbett, Denney, Fiske, and Walker,[3] it is necessary to take into account the fact that in very pure samples the measured resistivity change is not all due to a change in the bulk resistivity. Part of the change is due to a difference in the boundary scattering before and after irradiation. The impurity content of most of the samples used in these experiments was sufficiently high so that this effect was negligible.

IV. RESULTS

a. Production of Damage

We have measured the energy dependence of damage production in Al, Ni, Cu, Ag, Fe, Mo, and Ti. The resistance vs dose curves at constant bombarding energy were accurately linear for all these metals.

In Figs. 1 and 2 we give the experimental values of $(\Delta\rho/n)_e$ determined from Eq. (1), as a function of the average beam energy as determined from Eq. (19). In Figs. 3 and 4 we give values of $(\Delta\rho/n)_c$ as determined by Eq. (15) as a function of $\bar{E}$. For all elements, except Cu and Ag, the values $(\Delta\rho/n)_c$ differ from $(\Delta\rho/n)_e$

values only by the inclusion of the effects of angular deviation due to scattering. In the case of Cu and Ag, the effect of energy straggling was also taken into account in the manner outlined in the previous section.

All the data shown in Figs. 1 and 2 were obtained using liquid hydrogen as the refrigerant. In addition, we have values taken at the maximum energy using liquid helium as the refrigerant for the metals Ag, Cu, and Mo. All these show an increased damage production rate at the lower temperature, the enhancement being respectively 22%, 2.5%, and ~10%.

No data for Au, W, or Zn are shown in the above figures. As previously reported and discussed, $(\Delta\rho/n)_e$ in Au was $<2.5\times10^{-29}$ Ω cm per electron/cm² at a bombarding temperature of ~10°K, using 1.4-MeV electrons. In the case of W there was an initial increase of $\sim10^{-10}$ Ω cm during the first irradiation which was performed at liquid hydrogen. Subsequent prolonged irradiation at 20°K and a short irradiation at 4°K produced no further changes. After the initial increase, $(\Delta\rho/n)_e$ was $<2\times10^{-27}$ Ω cm per (electron/cm²) at both 20° and 4°K.

Two separate irradiated samples of Zn were studied at a bombarding temperature of 20°K. In both runs the control sample was observed to increase its resistivity with time. An experiment was performed in which the refrigerant was rapidly pumped past the samples with no beam current on. Both the irradiated and control samples increased in resistivity. It therefore seems likely that the samples were being plastically deformed by fluttering action in the refrigerant stream. One of the samples fractured after about one day, lending support to this idea. In spite of the variation of the control sample, it was possible to obtain some information about the effects of radiation. Both sample assemblies studied at liquid hydrogen showed an initial very large increase in resistivity for the irradiated sample as compared to the control sample. However, the resistivity change quickly saturated and at the end of the experiment it was impossible to measure any changes which could be attributed to the beam. In all these experiments we were changing the energy of the beam periodically in order to measure the energy dependence of damage production in a Ti sample which was included in the same sample assembly. It was not possible therefore to plot the resistivity change vs time at a single energy to see whether the Zn data fell on a smooth saturation curve. The initial resistivity change was $\sim3\times10^{-26}$ Ω cm per electron/cm² and at the end of the experiment $(\Delta\rho/n)_e$ was $\lesssim2\times10^{-27}$ Ω cm per electron/cm².

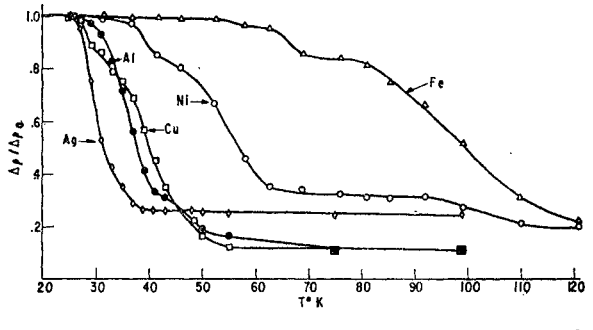

FIG. 5. Low-temperature recovery of electron-irradiated metals, bombarded at 20.4°K. The recovery curve is of the isochronal type, obtained by pulsing the samples to the specified temperatures and holding them there for 10 min. The samples are then quenched to 20.4°K for measurement.

b. Recovery

Recovery data starting at 20.4°K and extending up to room temperature were obtained for Al, Ni, Cu, Ag, Fe, and Mo. The control specimens of all these metals remained unaffected by the temperature cycling. Isochronal recovery curves of Al, Ni, Cu, Ag, and Fe in the temperature range from 20.4° to 120°K, are shown in Fig. 5. Recovery curves extending to room temperature are shown in Fig. 6. The low-temperature recovery of Mo is shown in Fig. 7. No further recovery in Mo was observed upon warming to room temperature.

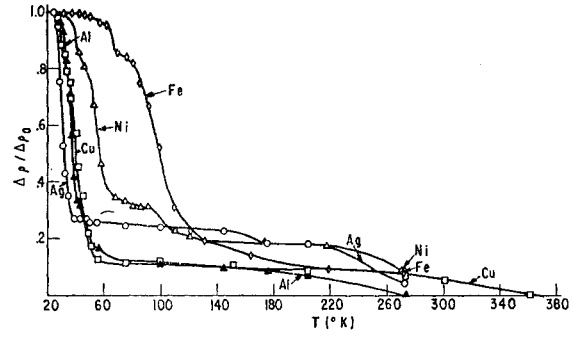

FIG. 6. Isochronal recovery curves extending to 0°C for various electron-irradiated metals, bombarded at 20.4°K.

Data below 20.4°K were also obtained for Ag, Cu, and Mo. In the case of Mo, a sample was irradiated at 4°K and raised directly to 20.4°K. About 10% recovery was observed. The total resistivity change at 4°K was quite low, however, and this number is only approximate. A detailed study of the Ag recovery below 20.4°K is shown in Fig. 8. This curve is a composite of two separate experiments; one using liquid helium as the refrigerant covering the range from 4° to 20°K, and the other using liquid hydrogen and covering the range above 20°K. Recovery data below 20°K in Cu have previously been published[4] and will not be presented here.

It was not possible to obtain extensive recovery data for Ti and Zn. In these metals the control samples were grossly affected by the temperature cycling. The changes induced in the samples by cycling greatly exceeded the initial changes produced by the radiation. Both Zn and Ti are hexagonal metals with anisotropic expansion coefficients. Since the samples are polycrystalline, this anisotropic expansion can give rise to

large stresses on individual grains. These individual grains then can deform plastically, leading to an increase in resistivity. It is probably necessary to work with single-crystal specimens in order to obtain recovery data in anisotropic metals. The Ti control sample remained constant during the early stages of the temperature cycle, and data obtained in this region are shown in Fig. 7.

All the recovery curves, except those for Mo and Ti, were obtained after a single bombardment at 1.4 MeV. They are thus characteristic of a unique bombarding energy. The Mo and Ti data on the other hand were taken after the samples had been bombarded at a number of different energies.

V. DETERMINATION OF THRESHOLD ENERGIES AND POINT DEFECT RESISTIVITIES

In this section we describe the determination of threshold energies and point defects resistivities. As has

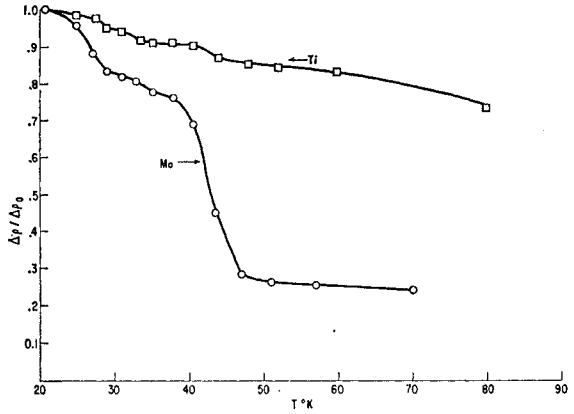

FIG. 7. Same as Fig. 5 for Mo and Ti. As explained in the text, the temperature range for Ti is restricted by the onset of changes due to the thermal cycling itself.

been said previously, it is impossible to compare the absolute value of cross section for atomic displacement with resistivity measurements without a knowledge of the resistivity of Frenkel pairs. Faced with this problem, we normalize at one energy and simply compare the predicted shapes of the cross section vs energy curves with experimental resistivity measurements. By trial and error we find a simple theoretical threshold function which gives the proper fit to the experimental data. This fit determines an "effective" threshold energy. If we then assume that the absolute value of the cross section computed from this effective threshold energy is correct, we can obtain absolute values of Frenkel pair resistivities.

In practice radiation damage calculations are divided into two parts. The first part of the calculation consists in evaluating the kinetic energies which are transferred to the lattice atoms. In the case of electrons the differential cross section for producing a recoil atom of energy T is given in the McKinley and Feshbach ap-

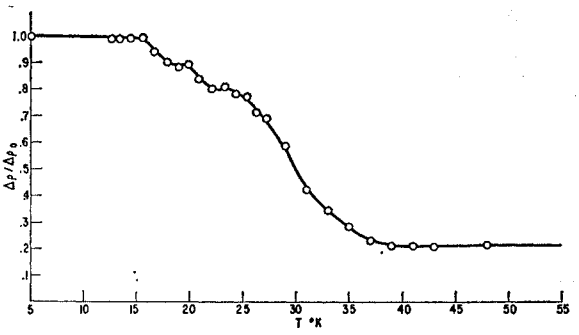

FIG. 8. Low-temperature isochronal recovery of electron-irradiated Ag. This is a composite curve constructed from two separate experiments, one of which covered the range up to 20°K and the other above 20°K.

proximation[12] by the formula

$$\frac{d\sigma}{dT}=(2.5\times10^{-25}\ \text{cm}^2)Z^2\frac{(1-\beta^2)}{\beta^4}\left(\frac{T_m}{T^2}\right)\times\left[1-\beta^2\frac{T}{T_m}+\pi\alpha\beta\left\{\left(\frac{T}{T_m}\right)^{\frac{1}{2}}-\frac{T}{T_m}\right\}\right], \quad (20)$$

where T_m is the maximum energy which can be transmitted to an atom by an incoming electron. The other symbols have their conventional meaning. Denoting the displacement probability of a primary recoil atom of energy T as $P_d(T)$, the total cross section for the production of primary displaced atoms is given by

$$\sigma_d=\int_{T_d}^{T_m}P_d(T)d\sigma(T). \quad (21)$$

T_d denotes the threshold energy for the onset of damage. In any particular direction in the crystal and at absolute zero temperature, $P_d(T)$ should be a simple step function equal to unity above T_d and zero below (see Fig. 9). However, T_d will be different in different crystal directions. Therefore, in a polycrystalline specimen, $P_d(T)$ should be a more complicated function starting from zero at T_d (now the threshold energy in the "easiest" crystal direction), but not reaching unity until some higher value of T. In order to facilitate calculation it is often assumed that the simple step function probability holds for all angles. The total cross section in this case is obtained by integrating Eq. (21) between T_d and T_m, giving

$$\sigma_d(\text{in cm}^2)=2.5\times10^{-25}Z^2\frac{(1-\beta^2)}{\beta^4}\times\left[\left(\frac{T_m}{T_d}-1\right)-\beta^2\ln\left(\frac{T_m}{T_d}\right)+\pi\alpha\beta\left\{2\left[\left(\frac{T_m}{T_d}\right)^{\frac{1}{2}}-1\right]-\ln\left(\frac{T_m}{T_d}\right)\right\}\right]. \quad (22)$$

[12] W. A. McKinley and H. Feshbach, Phys. Rev. 74, 12 (1948).

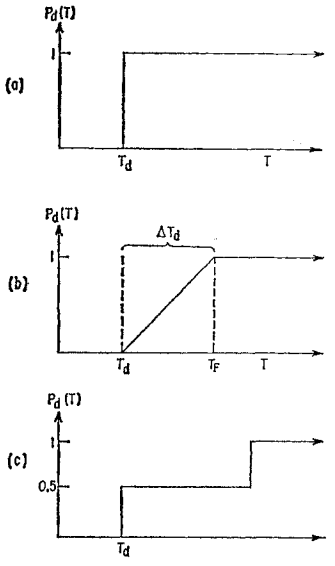

FIG. 9. Different forms for $P_d(T)$, the probability that a struck atom be displaced, as a function of the kinetic energy T transferred to the struck atom: (a) Step function, (b) linear function, (c) staircase function.

A different approximation is to assume that the function $P_d(T)$ rises linearly from T_d reaching unity at the higher value of T, T_F, and remaining constant thereafter (see Fig. 9). The total cross section is then given by

$$\sigma_d = 2.5\times 10^{-25}\frac{Z^2(1-\beta^2)}{\beta^4}\times\frac{T_m}{T_d}\left\{\left(1+\beta^2\frac{T_d}{T_m}\right)\ln\left(\frac{T_m}{T_d}\right)-\left[\frac{(T_m-T_d)}{T_m}(1+\beta^2)\right]+\pi\alpha\beta\left[2\left(1-\left(\frac{T_d}{T_m}\right)^{\frac{1}{2}}\right)+2\frac{T_d}{T_m}\left(1-\left(\frac{T_m}{T_d}\right)^{\frac{1}{2}}\right)+\frac{T_d}{T_m}\ln\left(\frac{T_m}{T_d}\right)-1+\frac{T_d}{T_m}\right]\right\}. \quad (23)$$

In discussing the comparison of linear or step $P_d(T)$ functions with experiment, it is useful to distinguish three different energy regions: low, intermediate, and high. At very low energies, close to the threshold for the onset of damage, the two different kinds of $P_d(T)$ functions give noticeably different relative cross section vs energy curves. As would be expected, the linear function gives a cross section curve which tails off more gradually towards lower energy. In principle, therefore, comparison with experiment should give some idea about the width ΔT_d of the displacement function. In practice, the differences are slight and only limited conclusions are possible. At intermediate energies, well above threshold, both linear and step functions, *which have $P=\frac{1}{2}$ at the same value of T*, give similar results for σ. This fact was first demonstrated by Corbett, Denney, Fiske, and Walker[4] and is illustrated explicitly in a number of calculations to be presented here. Thus the experimental results frequently do not distinguish between quite different $P_d(T)$ functions, and the threshold energies which are found by comparing theory to experiment must be interpreted as "effective" rather than true thresholds. At high energies, secondary defect production becomes important and the previous equations are no longer valid. Unfortunately, the range of energies available to us in these experiments is so restricted that we cannot cover the three energy regions for any one element. The energy region covered depends instead on the mass of the element in question. For example, Ag and Mo represent the low-energy case, Cu and Ni the intermediate case, and Al the high-energy case. We hope that our measurements will be extended by other investigators at both high and low energies.

The present experiments were undertaken in order to obtain an over-all picture of the variation of the basic damage parameters for a wide variety of metals. In most metals there is no prior theoretical basis for choosing a particular form of the displacement probability function or a value for the resistivity of Frenkel pairs. From these arguments, our method of comparing theory and experiment therefore should be expected to give only approximate values for threshold energies and point defect resistivities. However, in spite of the fact that these basic parameters are not determined precisely by our analysis, we believe that the analysis gives a reasonable over-all picture of their variation.

The threshold energies should be determined more closely than the resistivity values. We have already noted that the relative displacement cross section does not depend sensitively on the details of the displacement probability function. Hence it is valid to use simple functions to determine effective threshold energies. On the other hand, the resistivities which are deduced depend directly on the *absolute* values of the cross section which in turn depend more sensitively on the displacement functions chosen. However, in the case of copper, several independent estimates are available for the resistivity of Frenkel pairs which agree approximately with the value found here. This fact lends support to our approach.

Apart from the question of the absolute values of Frenkel pair resistivities, we expect that the values for

TABLE I. Effective threshold energies and Frenkel pair resistivities for various metals.

	Element	T_d (in eV)	$\Delta\rho_f$ (in $\mu\Omega$ cm/at.%)
fcc	Al	32	3.4
	Ni	24	3.2
	Cu	22	1.3
	Ag	28	1.4
	Au	>40	···
bcc	Fe	24	12.5
	Mo	37	4.5
	W	>35	···
Hexagonal	Ti	29	42

other metals *relative to copper* should be quite good. This is an important point for, as we shall show in a subsequent publication, there is a simple, systematic variation of the values we find for different elements. For the relative values to be reliable it is necessary only that the displacement probability functions for different elements have approximately the same shape as in copper.

In what follows we first discuss copper and then consider the other metals in turn. For most of the elements considered, the maximum atom recoil energy is sufficiently low so that we may neglect the secondary production of defects by the primary displaced atoms. This is not true for aluminum and it is necessary to take this secondary production into account in order to explain the results.

The values of threshold energies and point defect resistivities found by our analysis are summarized in Table I.

a. Threshold Energy and Frenkel Pair Resistivity in Copper

Normalized cross section curves calculated for several displacement probability functions are compared with values of $(\Delta\rho/n)_c$ in Fig. 10. A simple step displacement probability function with $T_d=22$ eV is seen to give excellent agreement with experiment in accord with previous measurements.[3] However, a linear function with $T_d=15$ and $T_F=30$ is seen to give an equally good fit. This illustrates the insensitivity of the calculated curves to the details of $P_d(T)$. Also shown are calculated curves for $T_d=22$ eV and $T_F=44$ and 80 eV respectively. These clearly disagree with experiment.

If we now take the absolute value of the total cross section which is calculated from the threshold curve with $T_d=22$ eV, we can obtain a value of $\Delta\rho_f$ from Eq. (15). In this manner we obtain $\Delta\rho_f=1.3$ $\mu\Omega$ cm per at.%. Comparison of this number with independent estimates is deferred until the end of this section.

Copper is unique in that there exists a detailed theory of the displacement behavior. Vineyard and his associates[13] at Brookhaven have performed detailed machine calculations of the dynamic response of a copper crystal when one of the atoms receives a fixed amount of kinetic energy in a specific crystal direction. Based on their early results, these authors estimated that the displacement probability function could be approximated by a slope function starting at $T_d=24$ eV and reaching unity at about 80 eV. This would correspond to curve 3 of Fig. 10 and does not agree with experiment. More recently[14] these authors have suggested that a better approximation may be a displacement function which rises abruptly at $T_d=24$ eV and then flattens out and then rises rather abruptly again at about 80 eV.

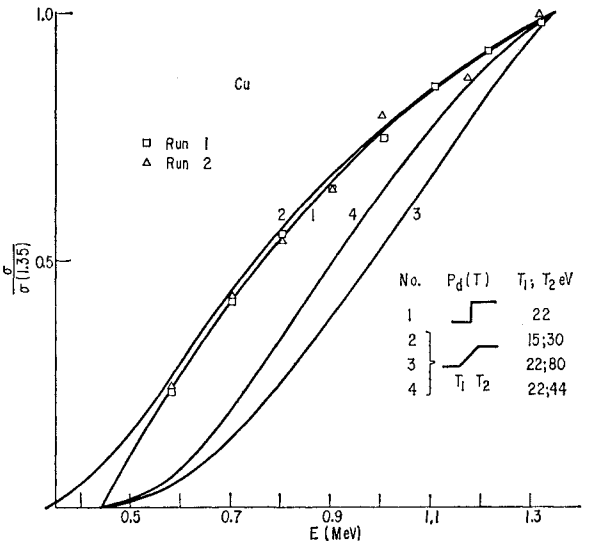

FIG. 10. Copper. Comparison of experimental data with theoretical curves of displacement cross section, normalized at 1.35 Mev, against bombarding electron energy. The squares and triangles are data points from two separate copper samples. The solid curves were calculated from the following displacement probability functions: (1) Step function $T_d=22$ eV; (2) Linear function $T_d=15$ eV, $T_F=30$ eV; (3) Linear function $T_d=22$ eV, $T_F=80$ eV; (4) Linear function $T_d=22$ eV, $T_F=44$ eV.

Cross-section calculations using such "staircase" functions (see Fig. 9) have previously been reported by Lucasson *et al.*[15] Several of these functions give an excellent fit with experiment.

Unfortunately, Vineyard *et al.* have not yet carried their calculations to the point where they can make a definite prediction for $P_d(T)$. Therefore we cannot say whether theory and experiment agree. The major uncertainty in the theory is the interatomic potential for atom separations in the range from 1 to 2Å. It is to be hoped that the comparison of the final results of the machine calculations with the measurements reported here will shed light on this interatomic potential. Other experiments which should eventually tie in with the detailed theory are the recovery spectra studied by Corbett, Smith, and Walker[4] and the single-crystal work reported in preliminary fashion by Cusson, Lucasson, and Walker.[16]

We consider now the comparison of the value of $\Delta\rho_f$ inferred here (1.3 $\mu\Omega$ cm per at.%) with independent values obtained by other investigators. There are two main ways of obtaining $\Delta\rho_f$. Firstly, one can calculate $\Delta\rho_f$ from theory. This has been done by a number of investigators and has resulted in a range of values. The lowest estimate is that due to Dexter[17] who gives 1.0

[13] J. B. Gibson, A. N. Goland, M. Milgram, and G. H. Vineyard, Phys. Rev. **120**, 1229 (1960).
[14] G. H. Vineyard, Discussions Faraday Soc. **31** (1961).
[15] A. Lucasson, P. Lucasson, and R. M. Walker, Berkeley Conference on Irradiated Materials, 1961 [Butterworth Scientific Publications Ltd., London (to be published)].
[16] Y. Cusson, P. Lucasson, and R. M. Walker, Berkeley Conference on Irradiated Materials, 1961 [Butterworth Scientific Publications Ltd., London (to be published)].
[17] D. L. Dexter, Phys. Rev. **87**, 768 (1952).

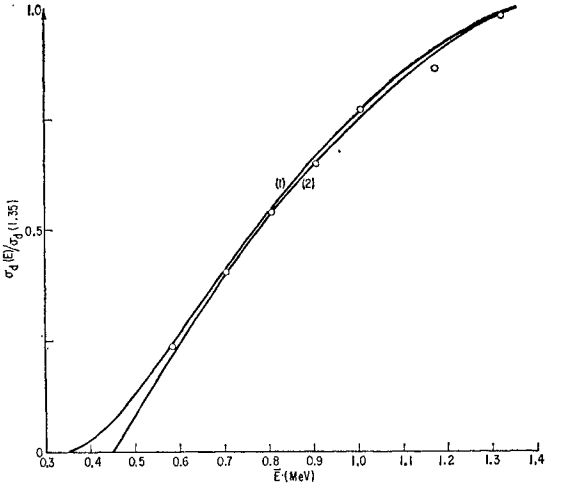

FIG. 11. Same as Fig. 10, for nickel. (1) Linear function $T_d=16$ eV, $T_F=32$ eV. (2) Step function $T_d=24$ eV.

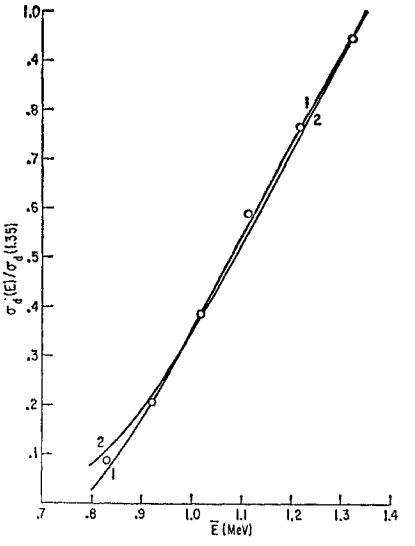

FIG. 12. Same as Fig. 10, for silver. (1) Step function $T_d=28$ eV. (2) Linear function $T_d=21$ eV, $T_F=42$ eV.

$\mu\Omega$ cm per at.%. The highest estimate is that due to Overhauser and Gorman[18] who give 12.0 $\mu\Omega$ cm per at.%.

The remaining method relies on a combination of theory and experiment. Some other physical property change is measured simultaneously with the resistivity change and the absolute number of defects is obtained from a theoretical estimate of this property change per defect. Stored energy, length, and lattice parameter have each been used as the independent physical property. Using a theoretical stored energy value of 4 eV per Frenkel pair[19–21] the electron damage results of Meechan and Sosin[22] give $\Delta\rho_f=3.0$ $\mu\Omega$ cm per at.% while the deuteron damage results of Granato and Nilan[23] give $\Delta\rho_f=2.1$ $\mu\Omega$ cm per at.%. The latter experiment was more accurate and hence this value is to be preferred. Using an atomic volume change of one per Frenkel pair, the lattice parameter measurement of Simmons and Balluffi[24] gives $\Delta\rho_f=2.4$ $\mu\Omega$ cm per at.%. Vook and Wert's[25] results on length change give a similar value.

These independent estimates are within a factor of 1.5 to 2 times the value inferred from the present measurements. We therefore feel that our method may be expected to give values for other metals with this accuracy. The discrepancy between our value and other estimates can easily be explained if the displacement probability function has the staircase shape suggested by Vineyard.[14] In this case, Lucasson *et al.* have shown by explicit calculation that the electron experiments yield $\Delta\rho_f$ values in accord with those obtained from the stored energy measurements.

It should be emphasized, however, that it is possible that the value derived from the present experiments is better than the other estimates. The values derived from the deuteron experiments are uncertain for two reasons. Firstly, the theoretical estimates of energy release and volume change per Frenkel pair are somewhat uncertain. Secondly, the deuteron damage includes clusters of defects as well as isolated Frenkel pairs. In neutron experiments, where the clusters are still more prevalent, the ratio of stored energy to resistivity is quite low.[26] Although the idea of a staircase displacement function brings the present results into line with the stored energy results and gives a consistent value of $\Delta\rho_f$ for all types of experiments, it is still not known whether this idea is correct.

To summarize our position, we feel that the value of $\Delta\rho_f$ determined by our analysis is probably good to within a factor of two and may be considerably better.

b. Nickel

Normalized experimental data and theoretical curves for an assumed step function of 24 eV and a linear function ranging from 16 to 32 eV are shown in Fig. 11. Both curves fit the data well. The value of $\Delta\rho_f$ inferred from the step function threshold is 3.2 $\mu\Omega$ cm per at.%.

c. Silver

Normalized experimental results for silver are compared with theory in Fig. 12. The experimental energies

[18] A. W. Overhauser and R. L. Gorman, Phys. Rev. **102**, 676 (1956).
[19] H. B. Hungtingon and F. Seitz, Phys. Rev. **61**, 315 (1942).
[20] L. Tewordt, Phys. Rev. **109**, 61 (1958); and private communication, 1960.
[21] E. Mann and A. Seeger, J. Phys. Chem. Solids **12**, 326 (1960).
[22] C. J. Meechan and A. L. Sosin, Phys. Rev. **113**, 424 (1959).
[23] T. G. Nilan and A. V. Granato, Phys. Rev. Letters **6**, 171 (1961).
[24] R. O. Simmons and R. W. Balluffi, Phys. Rev. **109**, 1142 (1958).
[25] R. Vook and C. Wert, Phys. Rev. **109**, 1529 (1958).
[26] T. H. Blewitt, R. R. Coltman, and C. E. Klabunde, Phys. Letters **3**, 132 (1959).

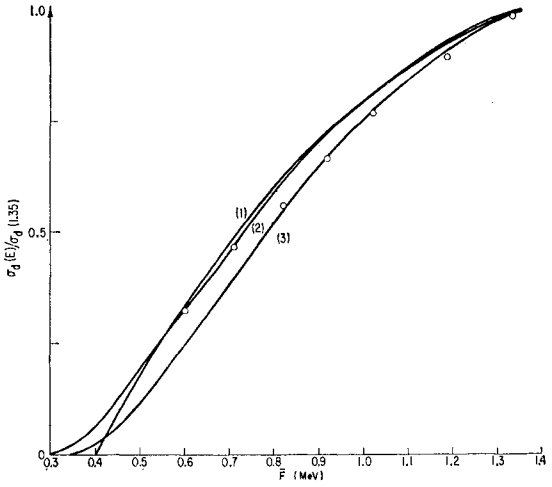

FIG. 13. Same as Fig. 10, for iron. (1) Step function $T_d=22$ eV. (2) Linear function $T_d=16$ eV, $T_F=32$ eV. (3) Linear function $T_d=18$ eV, $T_F=36$ eV.

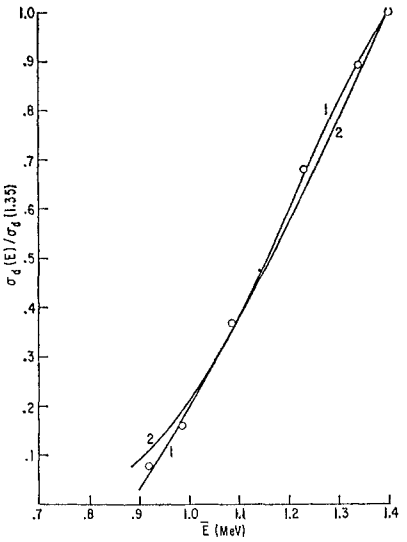

FIG. 14 Same as Fig. 10, for molybdenum. (1) Step function $T_d=37$ eV. (2) Linear function $T_d=28$ eV, $T_F=56$ eV.

extended below the onset threshold energy and hence covered a region where the variation in $P_d(T)$ might be expected to manifest itself. Curve 2 shows the best fit obtainable with a linear $P_d(T)$ function in which $T_F=2T_d$. Curve 1 shows the corresponding best fit for a simple step function with $T_d=28$ eV. Although the two curves are quite similar, the experimental data fall closer to curve 1 than they do to curve 2. The indication is therefore that the displacement probability function in Ag rises rather abruptly and does not vary rapidly over the range from T_d to $2T_d$. Following the same procedure previously outlined for Cu, $\Delta\rho_f$ is found to equal 1.4 $\mu\Omega$ cm per at.%.

d. Iron

Cross-section curves based on step and slope $P_d(T)$ functions are compared to experiment in Fig. 13. Although the agreement is reasonably good with an effective threshold energy of 24 eV, the fit is not as close as in the case of copper. As discussed by Lucasson *et al.*,[15] better agreement is obtained for more complicated staircase functions. Using a simple step threshold of 24 eV and proceeding as before we obtain a value of $\Delta\rho_f=12.5$ Ω cm per at.%. Using the staircase function which gave the best fit with experiment, Lucasson *et al.* obtained $\Delta\rho_f=19$ Ω cm per at.%.

e. Molybdenum

Molybdenum is similar to silver in that the experimental energies ranged below that for the onset of damage. The data and theoretical curves are shown in Fig. 14. Curve 1 was calculated for a step function of 37 eV and gives an excellent fit to the data. Curve 2 is the best fit for a linear function with $T_F=2T_d$ and does not fit the data as well as curve 1. As in the case of Ag, these results imply that $P_d(T)$ rises abruptly at the true threshold energy. The value of $\Delta\rho_f$ inferred from these data is 4.5 $\mu\Omega$ cm per at.%.

f. Titanium

Titanium is the only noncubic metal for which threshold data were obtained. Unfortunately, the very high residual resistivity of the sample precluded a detailed study of the production curve, and only a few points were obtained. Normalized experimental data and theoretical curves for an assumed step function of 29 eV and a linear function ranging from 19 to 38 eV are shown in Fig. 15. Although neither curve fits the data precisely, the step function gives a better fit. As in the case of the metals previously discussed, the indication is that the displacement probability function rises

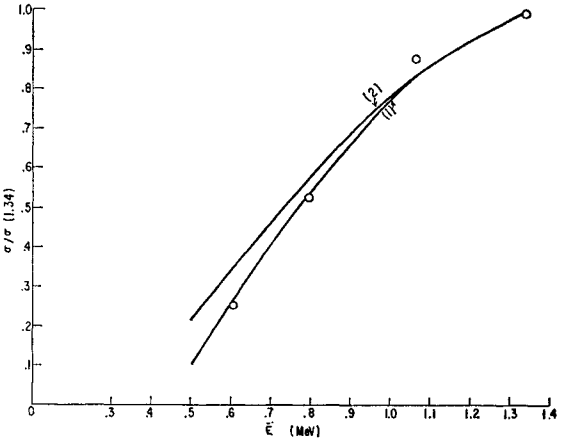

FIG. 15. Same as Fig. 10, for titanium. (1) Step function $T_d=29$ eV. (2) Linear function $T_d=19$ eV, $T_F=38$ eV.

fairly abruptly at the true threshold energy. The value of $\Delta\rho_f$ calculated from these data is 42 $\mu\Omega$ cm per at.%.

g. Aluminum

The Al sample was a wire 0.014 in. in diameter, and hence unlike other samples used which were all in the form of thin foils 0.001 in. thick. The wire was chosen in order to be able to compare the recovery results with the quenching data of DeSorbo and Turnbull[2] who used wire from the same spool. As a consequence of its large size, the observed voltage changes were small and the precision of the Al data was poor. The multiple scattering and energy loss corrections were also larger becuase of the large size. In applying these corrections, the Al wire was treated as a foil with a thickness equal to the average length of parallel lines drawn through a circle. The cylindrical geometry was therefore not taken into consideration explicitly. For these reasons, the present Al results must be viewed with reserve and a repetition of the experiment using thin foils would be desirable.

Normalized experimental data and calculated curves based on several different step displacement functions are shown in Fig. 16. It is clear that none of the calculated curves fit the data. It is possible that a slope function starting at around 20 eV and extending to 60 eV might fit, but such a displacement function would give a very large value for $\Delta\rho_f$. This seems unlikely and we have not pursued this approach. Instead, we have calculated production curves which include the process of secondary defect production by the primary recoils. This process can be neglected for the other elements but not for Al. The recoil energy of the light Al atoms is so high that the production curves are modified considerably by the secondary production.

In what follows we outline the procedures used in calculating the damage curves, including secondary defect production. The calculations were performed for several different assumptions concerning the damage process. The purpose of this work was twofold. Firstly, we were interested in seeing if the Al data could be satisfactorily explained on this basis. It may be questioned, however, whether the data justified this effort. A second reason we performed the calculations was to obtain a qualitative feeling for whether electron damage

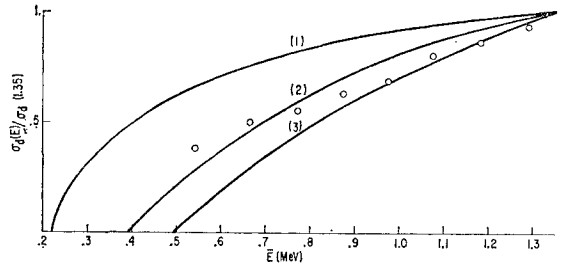

FIG. 16. Same as Fig. 10, for aluminum. (1) Step function $T_d=22$ eV. (2) Step function $T_d=45$ eV. (3) Step function $T_d=60$ eV.

experiments, at energies very much higher than threshold, could be used to obtain information about the details of the secondary production process. We therefore present the results of various calculations, including those which did not fit the experimental data.

If $G(T)$ is the total number of displaced atoms produced by a primary recoil, of energy T, then the total cross section for the production of displaced atoms is given by

$$\sigma_{\text{tot}}=\int_{T_d}^{T_m} G(T)dT. \tag{24}$$

Calculations were performed using five different assumptions concerning the displacement process. The calculations have four common assumptions. Firstly, the process is treated as a series of independent two-body collisions, and the crystal structure is ignored. Secondly, the atoms are treated as hard spheres; that is, all energy transfers up to the maximum energy are equally likely. Thirdly, a simple step displacement probability function is assumed. Finally, the primary recoil is assumed to lose an energy T_d in the displacement process.

The simplest calculation proceeds from the model of Kinchin and Pease.[27] This model embodies the following specific assumptions: (a) whenever a struck atom receives more than T_d it is considered displaced; (b) a secondary struck atom does not lose an energy T_d in being displaced but moves off with the full recoil energy; (c) whenever the energy of the striking atom falls below T_d it *replaces* the struck atom and is no longer displaced. With these assumptions, $G(T)$ is given by

$$\begin{aligned} &G(T)=1 \quad \text{for} \quad T<3T_d, \\ &G(T)=\tfrac{1}{2}[(T/T_d)-1] \quad \text{for} \quad T\geq 3T_d. \end{aligned} \tag{25}$$

For the case where $T_m<3T_d$ the total cross section is therefore still given by Eq. (22), when $T_m>3T_d$ the following expression holds:

$$\begin{aligned} \sigma_{\text{tot}}=2.5\times 10^{-25}\frac{Z^2(1-\beta^2)}{\beta^4}\Bigg\{&\frac{2T_m}{3T_d}-(\beta^2+\pi\alpha\beta)\ln 3 \\ &+2\pi\alpha\beta\left[\left(\frac{T_m}{T_d}\right)^{\frac{1}{2}}-\left(\frac{T_m}{3T_d}\right)^{\frac{1}{2}}\right] \\ &-\tfrac{1}{2}\Bigg[\left(\frac{T_m}{3T_d}\right)-1-\beta^2\ln\left(\frac{T_m}{3T_d}\right) \\ &+\pi\alpha\beta\{2[(T_m/3T_d)^{\frac{1}{2}}-1]-\ln(T_m/3T_d)\}\Bigg] \\ &+\frac{T_m}{2T_d}\Bigg[\ln\left(\frac{T_m}{3T_d}\right)-\left(1-\frac{3T_d}{T_m}\right)(\beta^2+\pi\alpha\beta) \\ &+2\pi\alpha\beta[1-(3T_d/T_m)^{\frac{1}{2}}]\Bigg]\Bigg\}. \end{aligned} \tag{26}$$

[27] G. H. Kinchin and R. S. Pease, *Reports on Progress in Physics* (The Physical Society, London, 1955), Vol. 18, p. 1.

In their review article, Seitz and Koehler[28] give a somewhat different treatment of the problem based on the following assumptions: (a) Whenever a struck atom receives more than the threshold energy it is displaced; (b) the recoil atom always loses an energy T_d when it is displaced; (c) replacement is neglected; that is, a striking atom is still counted as displaced even though its energy drops below T_d. The calculation in this case is somewhat more tedious as $G(T)$ is no longer an analytic function but must be evaluated numerically. We will refer to calculations based on the preceding assumptions as, "S-K, no replacement."

Following the procedure outlined by Seitz and Koehler, we have also performed calculations where assumption (c) above has been modified to include replacement in the same way as in the Kinchin and Pease model. These calculations are referred to as, "S-K, with replacement."

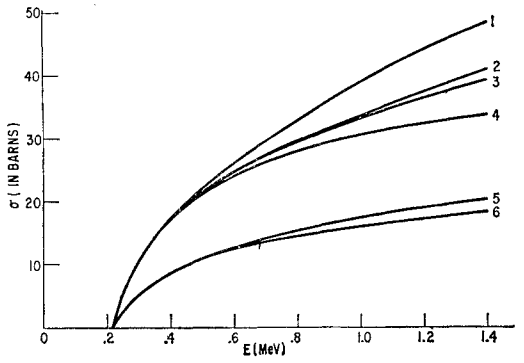

FIG. 17. Aluminum. Theoretical curves of displacement cross section against bombarding electron energy for various assumptions concerning the process of secondary defect production. All the curves are calculated assuming a step displacement function with $T_d=22$ eV. The following nomenclature, which distinguishes the various assumptions made in calculating the curves, is described in the portion of the text which discusses aluminum: (1) Seitz-Koehler, no replacement. (2) Kinchin-Pease. (3) Seitz-Koehler, with replacement. (4) No secondary production included. (5) $P=\frac{1}{2}$, no replacement. (6) $P=\frac{1}{2}$, with replacement.

Finally, we have performed calculations based on the Seitz and Koehler method where it has been assumed that the displacement probability function saturated at 0.5 instead of unity. These calculations are identified by the prefix, "$P=\frac{1}{2}$."

Figures 17 and 18 show the results of calculations for aluminum assuming a fixed threshold energy of 22 eV. With this threshold energy, the maximum electron energy plotted is 7 times the minimum energy for displacement. Thus, these curves should give some insight into what may be expected from electron bombardment experiments performed at energies very much higher than the threshold energy. Consider first Fig. 17 which gives the absolute magnitude of the cross sections. It

[28] F. Seitz and J. S. Koehler, *Solid-State Physics*, edited by F. Seitz and D. Turnbull (Academic Press Inc., New York, 1956), Vol. 2, p. 305.

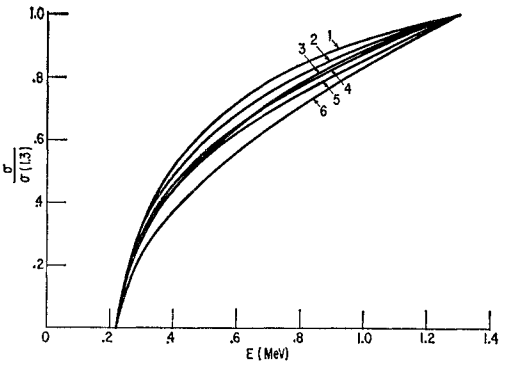

FIG. 18. Same curves as in Fig. 17, normalized at 1.3 Mev. (1) No secondary production included. (2) $P=7$, with replacement. (3) $P=7$, no replacement. (4) Seitz-Koehler, with replacement. (5) Kinchin-Pease. (6) Seitz-Koehler, no replacement.

should be noted first of all that the curves are quite smooth and do not possess large discontinuities which would serve to identify them experimentally. However, the curve for a simple step function without secondary production is well differentiated from the models which incorporate the secondary production. Of these models, S-K no replacement, gives the highest cross section. The Kinchin and Pease model lies somewhat lower and gives practically the same results as S-K with replacement. As would be expected, the $P=\frac{1}{2}$ calculations give the lowest production rates. It would appear from these curves that, *if the absolute number of defects which are produced can be measured precisely*, then some information can be obtained about the secondary production process. Much more information could be obtained if the secondary defects lay so close to the primary defect, that an experimentally measurable, *multiple defect* were formed. Unfortunately, in the present experiments we are unable to measure the absolute number of defects or to single out the multiple defects for study. We must therefore normalize the calculations at one energy as shown in Fig. 18. In such a plot, the various theoretical curves lie closer together and the effects of secondary production are less pronounced.

In the foregoing we have discussed how the cross sections curves are altered by secondary defect production when the maximum electron energy is high with respect to the threshold energy. As the threshold energy approaches the maximum energy any differences will disappear. In order to get a picture of this change we have calculated curves using two different threshold energies for the Kinchin and Pease model. The results are shown in Fig. 19. It can be seen that for $T_d=22$ the inclusion of the secondary defects considerably alters the results. At $T_d=45$ eV, however, the differenence is quite small. The ratio of the maximum recoil energy to the threshold energy is ~ 11 in the first case, and ~ 5 in the second. It would appear that it is necessary to obtain ratios of this order before the inclusion of

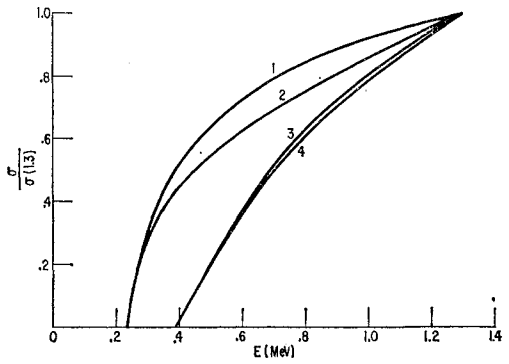

FIG. 19. Aluminum. Comparison of theoretical curves, with and without secondary defect production, for two different threshold energies. (1) No secondary production; (2) Kinchin and Pease model (both with $T_d=45$ eV). (3) No secondary production; (4) Kinchin and Pease model (both with $T_d=45$ eV).

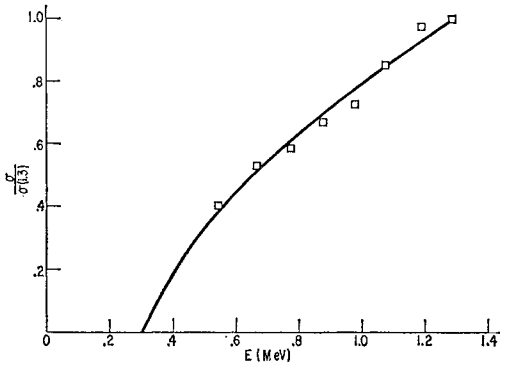

FIG. 20. Aluminum. Comparison of experimental data with a theory which includes secondary defect production. The solid curve is calculated from the Seitz-Koehler, no replacement model with $T_d=32$ eV.

secondary defect production substantially alters the shape of the normalized cross-section curve.

None of the curves calculated above actually fit the experimental data. Working with the S-K, no replacement model, we were able to obtain satisfactory agreement with experiment using a value of $T_d=32$ eV. The extent of agreement is shown in Fig. 20. Using the absolute value of the cross section calculated from the above model we obtain a value of $\Delta\rho_f=3.4$ $\mu\Omega$ cm per at.%. This is close to the value obtained by Balluffi and Simmons[29] for single vacancies and suggests, as in the case of copper, that the values of $\Delta\rho_f$ derived from our analysis are low by about a factor of two.

As previously noted, an underlying assumption in all the calculations discussed above is that the crystal structure plays no role, and that the secondary production process can be treated as a series of independent two-body collisions. However, Silsbee[30] has shown theoretically that the crystal structure may be important, and that the correlated nature of successive collisions can "focus" energies into particular crystal directions. The importance of this effect is not known in Al but it is clear that the secondary production models should not be taken too literally. It may turn out that one of these models provides a useful tool for calculation, but the complete elucidation of the relation of these models to what actually goes on in an irradiated crystal needs further development.

We would like to make one final point concerning the Al data. Although we have drawn a smooth curve through the experimental points, there is a suggestion of a break in the data around 1 MeV as if some new process were setting in. However, a calculation based on the assumption that a new defect is produced at a threshold energy of 150 eV (corresponding to an electron energy of 1.0 MeV) shows that this would not give a discernible break in the production curve. We feel, therefore, that the smooth curve is probably correct.

[29] R. O. Simmons and R. W. Balluffi, Phys. Rev. 117, 52 (1960).
[30] R. H. Silsbee, J. Appl. Phys. 28, 1246 (1957).

VI. SUMMARY

In this paper we have presented results for electron-bombardment induced changes in residual electrical resistance for the metals Al, Ag, Au, Cu, Fe, Mo, Ni, Ti, W, and Zn. The changes were measured as a function of electron energy in the range from 0.5 to 1.4 MeV. Most of the bombardments were performed at 20.4°K. Following irradiation the thermal recovery of the induced change was measured up to room temperature.

No damage was observed in W or Au thus setting lower limits on the threshold energy for damage production of 35 and 40 eV, respectively. Zinc showed an anomalous behavior in that the added resistivity was not a linear function of dose at a fixed bombarding energy. For all the other metals studied the damage production curves were accurately linear.

The slopes of these production curves were plotted against bombarding electron energy and then compared with theoretical curves calculated from simple displacement theory. The agreement between theory and experiment was excellent and the values found are shown in Table I. Due to the method of analysis these values are lower limits to the correct values. Arguments were presented to show that the correct values are probably not more than twice these lower limits.

In the case of Al it was necessary to take secondary defect production into account in order to get agreement with experiment. In the discussion of the Al data a number of representative curves were included showing the general effects of including secondary defect production.

The recovery curves for all the metals for which it was possible to obtain data showed a pronounced low-temperature recovery stage analogous to the extensively studied stage-I recovery in copper. All the metals studied also showed a pronounced substructure in the stage-I recovery.

The threshold energies, point defect resistivities, and recovery temperatures show a systematic behavior for the set of elements studied. This systematic behavior will be discussed in a future publication.